



HAL
open science

Abundance ratios in dwarf elliptical galaxies

Ş. Şen, R. F. Peletier, A. Boselli, M. den Brok, J. Falcón-Barroso, G. Hensler,
J. Janz, E. Laurikainen, T. Lisker, J. J. Mentz, et al.

► **To cite this version:**

Ş. Şen, R. F. Peletier, A. Boselli, M. den Brok, J. Falcón-Barroso, et al.. Abundance ratios in dwarf elliptical galaxies. *Monthly Notices of the Royal Astronomical Society*, 2018, 475, pp.3453-3466. 10.1093/mnras/stx3254 . insu-03666273

HAL Id: insu-03666273

<https://insu.hal.science/insu-03666273>

Submitted on 12 May 2022

HAL is a multi-disciplinary open access archive for the deposit and dissemination of scientific research documents, whether they are published or not. The documents may come from teaching and research institutions in France or abroad, or from public or private research centers.

L'archive ouverte pluridisciplinaire **HAL**, est destinée au dépôt et à la diffusion de documents scientifiques de niveau recherche, publiés ou non, émanant des établissements d'enseignement et de recherche français ou étrangers, des laboratoires publics ou privés.

Abundance ratios in dwarf elliptical galaxies

Ş. Şen,^{1,2★} R. F. Peletier,^{1★} A. Boselli,³ M. den Brok,⁴ J. Falcón-Barroso,^{5,6}
 G. Hensler,⁷ J. Janz,^{8,9,10} E. Laurikainen,⁹ T. Lisker,¹¹ J. J. Mentz,^{1,12} S. Paudel,¹³
 H. Salo,⁹ A. Sybilka,¹⁴ E. Toloba,¹⁵ G. van de Ven,¹⁶ A. Vazdekis^{5,6}
 and C. Yesilyaprak²

¹Kapteyn Astronomical Institute, University of Groningen, PO Box 800, NL-9700 AV Groningen, Netherlands

²Department of Astronomy and Astrophysics, Faculty of Science, Ataturk University, 25030 Erzurum, Turkey

³Aix Marseille Université, CNRS, LAM (Laboratoire d'Astrophysique de Marseille), UMR 7326, F-13388 Marseille, France

⁴Institute for Astronomy, ETH Zurich, Wolfgang-Pauli-Strasse 27, CH-8093 Zurich, Switzerland

⁵Instituto de Astrofísica de Canarias, Calle Vía Láctea s/n, E-38200 La Laguna, Tenerife, Spain

⁶Departamento de Astrofísica, Universidad de La Laguna, E-38205 La Laguna, Tenerife, Spain

⁷Department of Astrophysics, University of Vienna, Türkenschanzstrasse 17, A-1180 Vienna, Austria

⁸Centre for Astrophysics and Supercomputing, Swinburne University, Hawthorn, VIC 3122, Australia

⁹Astronomy Research Unit, University of Oulu, FI-90014 Oulu, Finland

¹⁰Finnish Centre of Astronomy with ESO (FINCA), University of Turku, Väisäläntie 20, FI-21500 Piikkiö, Finland

¹¹Astronomisches Rechen-Institut, Zentrum für Astronomie der Universität Heidelberg, Mönchhofstraße 12-14, D-69120 Heidelberg, Germany

¹²Center for Space Research, North-West University, Potchefstroom 2520, South Africa

¹³Department of Astronomy and Center for Galaxy Evolution Research, Yonsei University, Seoul 03722, Republic of Korea

¹⁴European Southern Observatory, Karl-Schwarzschild-Strasse 2, D-85748 Garching bei München, Germany

¹⁵University of the Pacific, Department of Physics, 3601 Pacific Avenue, Stockton, CA 95211, USA

¹⁶Max-Planck-Institut für Astronomie, Königsstuhl 17, D-69117 Heidelberg, Germany

Accepted 2017 December 12. Received 2017 December 11; in original form 2017 April 20

ABSTRACT

We determine abundance ratios of 37 dwarf ellipticals (dEs) in the nearby Virgo cluster. This sample is representative of the early-type population of galaxies in the absolute magnitude range $-19.0 < M_r < -16.0$. We analyse their absorption line-strength indices by means of index–index diagrams and scaling relations and use the stellar population models to interpret them. We present ages, metallicities, and abundance ratios obtained from these dEs within an aperture size of $R_e/8$. We calculate $[\text{Na}/\text{Fe}]$ from NaD, $[\text{Ca}/\text{Fe}]$ from Ca4227, and $[\text{Mg}/\text{Fe}]$ from MgB. We find that $[\text{Na}/\text{Fe}]$ is underabundant with respect to solar, whereas $[\text{Mg}/\text{Fe}]$ is around solar. This is exactly opposite to what is found for giant ellipticals, but follows the trend with metallicity found previously for the Fornax dwarf NGC 1396. We discuss possible formation scenarios that can result in such elemental abundance patterns, and we speculate that dEs have disc-like star formation history (SFH) favouring them to originate from late-type dwarfs or small spirals. Na-yields appear to be very metal-dependent, in agreement with studies of giant ellipticals, probably due to the large dependence on the neutron-excess in stars. We conclude that dEs have undergone a considerable amount of chemical evolution, they are therefore not uniformly old, but have extended SFH, similar to many of the Local Group galaxies.

Key words: galaxies: abundances – galaxies: clusters: individual: Virgo – galaxies: dwarf – galaxies: evolution – galaxies: stellar content.

1 INTRODUCTION

Early-type dwarf galaxies (dEs) play a key role in understanding galaxy cluster evolution. dEs,¹ the low-luminosity ($M_B > -18$)

and low-surface-brightness ($\mu_B > 22$ mag arcsec⁻²) population of the early-type galaxy (ETG) class, are found in high-density environments and are very rare in isolation (Gavazzi et al. 2010; Geha et al. 2012; Blanton et al. 2005). dEs are found abundantly in groups and clusters of galaxies where they dominate in numbers (Binggeli, Sandage & Tammann 1988).

The Lambda cold dark matter (CDM) hierarchical merging scenario predicts that CDM haloes are formed because of gravitational instabilities and evolve hierarchically via mergers (White & Rees

* E-mail: s.sen@rug.nl (SS); peletier@astro.rug.nl (RFP)

¹ The term dE has traditionally been used to refer to dwarf elliptical galaxies, whereas we loosely use the term here to include dwarf ellipticals and dwarf lenticulars (dSO).

1978; Frenk et al. 1988; White & Frenk 1991; Lacey & Cole 1993; Cole et al. 2000). These models predict that dwarf-size dark matter haloes form first and then merge forming more massive haloes.

The class of dEs contains objects covering a wide range of internal properties, with sometimes rather complicated structures. Taking advantage of deep photometric studies, we know that several of them contain substructures such as discs, spiral arms and irregular features (e.g. Jerjen, Kalnajs & Binggeli 2000; Barazza, Binggeli & Jerjen 2002, De Rijcke et al. 2003; Geha et al. 2003; Graham & Guzmán 2003; Ferrarese et al. 2006; Lisker et al. 2006a; Janz et al. 2012, 2014). Apart from this, dEs also show a complicated variety of internal kinematics and dynamics. dEs with similar photometric properties can have different stellar populations (Michielsen et al. 2008; Paudel et al. 2010; Koleva et al. 2009, 2011; Ryś et al. 2015) and different rotation speeds (Geha, Guhathakurta & van der Marel 2002; Pedraz et al. 2002; Simien & Prugniel 2002; Geha et al. 2003; van Zee, Barton & Skillman 2004; Chilingirian 2009; Koleva et al. 2009, 2011; Toloba et al. 2009, 2011, 2014b, 2015; Ryś, Falcón-Barroso & van de Ven 2013; Ryś, van de Ven & Falcón-Barroso 2014). Kormendy (1985) suggested that they developed their spheroidal non-star forming appearance, which is probably highly flattened (Lisker et al. 2006a, 2007), during a transformation from a late-type galaxy that fell into a cluster; it is thought that this transformation is induced by the environment because the morphology–density relation largely depends on the environment (e.g. Boselli & Gavazzi 2014).

Processes for that transformation include ram-pressure stripping (Gunn & Gott 1972; Lin & Faber 1983) and galaxy harassment (Moore, Lake & Katz 1998). Ram-pressure stripping should be able to remove the galaxy’s remaining gas from the system on short time-scales, so that star formation stops quickly. The effect of ram-pressure stripping depends strongly on the density of the environment, and it is expected that their angular momentum and structure should be preserved (Ryś et al. 2014) while galaxy harassment by tidal interactions between a galaxy and the potential of the cluster can heat up the object, increasing the velocity dispersion, slow its rotation down and remove stellar mass so that discs are transformed into more spheroidal objects (Moore et al. 1998). In this case, a galaxy can lose some of its intrinsic angular momentum. For a more detailed review on these effects, see Boselli & Gavazzi (2006, 2014).

How exactly ram-pressure stripping and harassment transform objects is still rather unclear. Ryś et al. (2013) concluded that a transformation mechanism should be able to not only lower the angular momentum but also increase the stellar concentration of dEs compared to their presumed progenitors. Toloba et al. (2015) show that even a combination of these two mechanisms cannot easily remove all of the angular momentum, something which is needed to explain some observations. Since ram-pressure stripping is happening on short time-scales, it might be a standard mechanism to transform late type star-forming galaxies into dwarf ETGs. After being in the cluster for a long time, the galaxy goes through its centre several times, during which it can heat up, lose stellar rotation and also lose its discy structure. Since fast rotators in the outer parts of the cluster are rotating faster than the fast rotators found in the inner part of the cluster (Toloba et al. 2014a, hereafter T14), Springel et al. (2005) suggested that clusters were formed by the accretion of small groups of galaxies. According to this scenario, the properties of slow and non-rotating dEs in the centre of the cluster as well as the existence of kinematically decoupled cores observed in some of the SMAKCED (Stellar content, MASS and Kinematics of Cluster Early-type Dwarfs) dEs (Toloba et al.

2014b) can be explained. Therefore, galaxy clusters, as a place with many dwarf ellipticals with a range of environmental properties, are excellent places to study the evolution and formation of the dEs.

Not only can be used the morphology, or their kinematics, to study the evolution of galaxies: More detailed information can be obtained by studying the stellar populations, since the distribution of ages, metallicities, and abundance ratios provide important information that can be used to study the evolutionary history of galaxies since chemical abundances of the gas are locked into the stars when they form. This information can be obtained via two general techniques. The first is by studying ages and abundances from observations of individual stars, which can be done for nearby galaxies where individual stars can be resolved. The second is by studying the integrated light from more distant galaxies to derive star formation histories (SFHs) and abundance distributions. This second technique is the only one currently available for galaxies at the distance of the Virgo cluster (16.5 Mpc, Mei et al. 2007).

A non-trivial problem when analysing the spectra of galaxies is the degeneracy between age and metallicity. One can break the age-metallicity degeneracy using a wide wavelength baseline, a combination of line indices, and accurate data. These then are compared to evolutionary stellar population models (e.g. Vazdekis 1999; Bruzual & Charlot 2003; Thomas, Maraston & Bender 2003; Maraston 2005; Schiavon 2007; Maraston et al. 2009; Vazdekis et al. 2010; Conroy & van Dokkum 2012). By comparing model predictions with observational galaxy parameters age and metallicity distributions of the stars in that galaxy can be obtained. One can compare observations with models of a single age and metallicity, obtaining SSP-equivalent parameters. More complicated approaches, [e.g. STECKMAP (Ocvirk et al. 2006), STARLIGHT (Cid Fernandes et al. 2005)] provide full SFHs. A problem still remains the unicity of the solutions. As a rule of thumb, one can say that the larger the wavelength range is, the more unique the solution.

Stellar population studies show that dEs have on average a lower metal content than giant ellipticals, as expected from the metallicity–luminosity relation (Skillman, Kennicutt & Hodge 1989; Michielsen et al. 2008; Sybilaska et al. 2017). Their ages are somewhat younger on average. However, recent studies show that the stellar populations of dEs show indications of both young and old ages and a range in gradients (e.g. Koleva et al. 2009, 2011; den Brok et al. 2011; Ryś et al. 2015). Studies about detailed abundance ratios in dEs are scarce. Gorgas et al. (1997); Michielsen et al. (2008) and Sybilaska et al. (2017) show that [Mg/Fe] is similar to solar, lower than what is found in giant ellipticals. [Mg/Fe] can, however, provide important information about the formation of a galaxy. Individual galaxy abundances are the result of chemical evolution, involving element enrichment in stars, supernova explosions, and galactic winds from, for example, AGB stars. As a result, the measurement of abundances of many elements can give us a very detailed picture of the formation and evolution of a galaxy (see e.g. Tolstoy, Hill & Tosi 2009 for Local Group galaxies). We often call this way of studying galaxies galactic archaeology.

Measured abundances of various elements allow us, in principle, to understand which enrichment processes have been dominant at different epochs of galaxy formation because of their different nucleosynthetic origin. It is thought that a group of lighter elements, the so called α -elements, such as O and Mg, are produced by type II supernovae (SNe II), supernovae originated from massive stars, which therefore occur on short time-scales (Worthey, Faber &

Gonzalez 1992). Most of the Fe, on the other hand, is predominantly produced by a different group of supernovae, those of type Ia (SNe Ia), which occur on a much longer time-scale. As a result, elemental ratios of $[\alpha/\text{Fe}]$ give us information about the relative contribution from the two types of supernovae at a given time, i.e. about the time-scale of star formation. The observed correlation of $[\alpha/\text{Fe}]$ abundance ratio and galaxy mass is an indication of the downsizing (Vazdekis, Trujillo & Yamada 2004; Nelan et al. 2005; Thomas et al. 2005). For dEs, Gorgas et al. (1997) measured that Virgo dEs are consistent with solar $[\alpha/\text{Fe}]$ abundance ratio and showed that star formation must have happened on longer time-scales in these systems. Several works confirmed these results and found that dEs have younger ages and lower metallicities than normal Es (Geha et al. 2003; van Zee et al. 2004). Interpretation of abundance ratios of other elements is more complicated, and has been limited mostly to the Local Group. They are also used to obtain a more detailed picture and information on the initial mass function (IMF) and star formation history (McWilliam 1997). In dEs, at the moment, very little information is available on abundance ratios of elements (apart from Mg and Fe), mainly because of the lack of high signal-to-noise (S/N) spectra, but also because of the lack of methods to analyse them. Since this has changed in recent years, we have been able to start a program to obtain and analyse abundance ratios in dwarf ellipticals. The results on the pilot galaxy NGC 1396 are presented in Mentz et al. (2016). In this paper, a sample of 37 galaxies from the SMAKCED sample is analysed.

To determine the abundance ratios from integrated spectra, we use the hybrid model calibration by Conroy, Graves & van Dokkum (2014, hereafter CvD). They calculate spectra using standard stellar population models with solar abundance ratios, which are modified by using theoretical responses of spectra to abundance ratio variations, following a method developed by Walcher et al. (2009). Here, we will study the abundance ratios of a few elements in dwarf ellipticals, obtaining data that allow us to compare the formation history of dEs with those of giant ellipticals, the Milky Way, and other galaxies of the Local Group. We will focus on the Na doublet absorption features in the optical wavelength range at 5890 and 5896 Å (NaD hereafter) and the Ca4227 line-strength indices, to study the abundances of Na and Ca, as well as the better studied Mg. Although interpreting the observational results is at present extremely difficult, already many conclusions can be derived by comparing them to other types of galaxies.

This work is part of the SMAKCED project, aimed at studying the nature of dEs in the Virgo Cluster. More details about the galaxies discussed here, and their properties, can be found in the other SMAKCED papers (Janz et al. 2012, 2014; Toloba et al. 2014b, 2014a, 2015). In Toloba et al. (2014a), a description is given of the spectroscopic part of the survey, whereas the H-band photometry is described in Janz et al. (2014). In Toloba et al. (2014a), kinematics of two dEs are presented that show kinematically decoupled cores. In Toloba et al. (2015), the stellar kinematics of dEs are presented as a function of projected distance to the centre of the Virgo cluster.

The Virgo cluster is an ideal laboratory to study dEs because it contains hundreds of them, is close enough to resolve their detailed structure, and is a dynamically young cluster that is still evolving today (Binggeli, Popescu & Tammann 1993; Boselli et al. 2014). In this paper, we focus on the abundance ratio distribution of dEs and compare them with other types of galaxies.

This paper is organized as follows. In Section 2, we present the general properties of our samples, the observations, and the main data reduction steps. We describe the measurements of age-sensitive and metallicity-sensitive Lick indices. In Section 3, we derive the

ages and metallicity based on the Lick indices and the abundance ratios. In Section 4, our results are summarized and discussed. In Section 5, conclusions are given.

2 OBSERVATIONS AND DATA REDUCTION

Our sample consists of 37 galaxies, the full spectroscopic sample of the SMAKCED project. For each of them, we obtained data suitable for a detailed stellar population study, with relatively high spectral resolution and high S/N ratio. Two galaxies in the sample (VCC1684 and VCC2083) were not included, since no ages could be determined because of lack of observed Balmer lines. The spectroscopic data were obtained at three different telescopes. A total of 26 dEs were observed at the 4.2-m William Herschel Telescope (WHT) using the double-arm ISIS spectrograph, of which the blue-arm covered the wavelength range 4200–5000 Å and the red-arm covered the wavelength range 5500–6700 Å. A total of 10 dEs were observed at the 2.5-m Isaac-Newton Telescope (INT), using the IDS spectrograph covering the wavelength range 4600–5600 Å, whereas the remaining three dEs were observed at the 8-m Very Large Telescope (VLT), using the FORS2 spectrograph that covers the wavelength range 4500–5600 Å.

Table 1 summarizes the main properties of these 37 dEs (see also T14).

The data were reduced following the standard procedure for long-slit spectra using the package REDUCEME (Cardiel 1999). Details on sample selection, observations, and data reduction are presented in T14.

2.1 Line-strength measurements

Observed spectral data can be studied either by fitting the full spectrum or by focusing on selected line indices. In this work, we study selected line indices. We measured Lick indices (Worthey et al. 1994) in the Line Index System (LIS)-5 Å flux calibrated system (Vazdekis et al. 2010). The new LIS has numerous advantages over the Lick system. It is defined at three different resolutions, namely 5.0 Å, 8.4 Å, and 14.0 Å. As such, it is particularly useful for analysing small galaxies and globular clusters. As the resolution of the Lick/IDS library (FWHM \sim 8–11 Å) is much lower than what is available with our high resolution spectra, we broadened the spectra to the LIS-5 Å system. The LIS-5 Å system choice expresses a factor of 2 improvement in resolution over Lick/IDS system. Also, the fact that the LIS system is flux calibrated makes it easier to reproduce data from other authors.

The spectra were broadened to the LIS-5 Å system, taking into account the velocity dispersion of the spectra. This ensures that every galaxy spectrum has the same spectral resolution, which is important and necessary to compare them with each other.

We measured a total of 23 Lick indices (Faber et al. 1985; Gorgas et al. 1993; Worthey et al. 1994, Worthey & Ottaviani 1997). In this paper, we use $H\gamma_F$, $H\beta$, Fe4383, Fe4531, Fe5270, Fe5335, Fe5406, Fe5709, Mg β , Ca4227, and NaD. The summary of the indices used is tabulated Table 2. However, because of the different wavelength range covered by our spectra, not all lines are used for all galaxies. Galaxies observed at the VLT do not cover the $H\gamma_F$, Fe4383, and NaD lines. Also, in some spectra that are obtained by WHT, $H\beta$ is located at the end of the spectrum, and since the spectra suffer from vignetting there, we could not determine this index here. In Tables 3 and 4, we show the line-strength index measurements for each galaxy used.

Table 1. Properties of the SMAKCED dEs. Column 1: galaxy name. Columns 2 and 3: right ascension and declination in J2000, respectively. Columns 4 and 5: r -band magnitude (in the AB system) and half-light radius by Janz & Lisker (2008, 2009), respectively. Column 6: velocity dispersion.

Galaxy	RA (J2000)	Dec (J2000)	M_r (mag)	R_e (arcsec)	σ_e (km s ⁻¹)
VCC0009	12:09:22.25	13:59:32.74	-18.2	37.2	26.0 ± 3.9
VCC0021	12:10:23.15	10:11:19.04	-17.1	15.2	28.9 ± 2.9
VCC0033	12:11:07.79	14:16:29.19	-16.9	09.8	20.8 ± 4.9
VCC0170	12:15:56.34	14:26:00.33	-17.6	31.3	26.6 ± 4.6
VCC0308	12:18:50.90	07:51:43.38	-18.0	18.6	24.1 ± 2.4
VCC0389	12:20:03.29	14:57:41.70	-18.1	18.0	30.9 ± 1.2
VCC0397	12:20:12.18	06:37:23.51	-16.8	13.6	35.7 ± 1.9
VCC0437	12:20:48.10	17:29:16.00	-18.0	29.5	40.9 ± 4.0
VCC0523	12:22:04.14	12:47:14.60	-18.7	26.1	42.2 ± 1.0
VCC0543	12:22:19.54	14:45:38.59	-17.8	23.6	35.1 ± 1.4
VCC0634	12:23:20.01	15:49:13.25	-18.5	37.2	31.3 ± 1.6
VCC0750	12:24:49.58	06:45:34.49	-17.0	19.5	43.5 ± 2.9
VCC0751	12:24:48.30	18:11:47.00	-17.5	12.3	32.1 ± 2.4
VCC0781	12:25:15.17	12:42:52.59	-17.2	13.4	38.0 ± 2.8
VCC0794	12:25:22.10	16:25:47.00	-17.3	37.0	29.0 ± 3.9
VCC0856	12:25:57.93	10:03:13.54	-17.8	16.5	31.3 ± 4.1
VCC0917	12:26:32.39	13:34:43.54	-16.6	09.9	28.4 ± 1.4
VCC0940	12:26:47.07	12:27:14.17	-17.4	19.8	40.4 ± 1.3
VCC0990	12:27:16.94	16:01:27.92	-17.5	10.2	38.7 ± 1.3
VCC1010	12:27:27.39	12:17:25.09	-18.4	22.2	44.6 ± 0.9
VCC1087	12:28:14.90	11:47:23.58	-18.6	35.4	42.0 ± 1.5
VCC1122	12:28:41.71	12:54:57.08	-17.2	17.3	32.1 ± 1.7
VCC1183	12:29:22.51	11:26:01.73	-17.9	21.1	44.3 ± 2.4
VCC1261	12:30:10.32	10:46:46.51	-18.5	23.8	44.8 ± 1.4
VCC1304	12:30:39.90	15:07:46.68	-16.9	16.5	25.9 ± 2.7
VCC1355	12:31:20.21	14:06:54.93	-17.6	30.3	20.3 ± 4.7
VCC1407	12:32:02.73	11:53:24.46	-17.0	12.1	31.9 ± 2.1
VCC1431	12:32:23.41	11:15:46.94	-17.8	09.8	52.4 ± 1.6
VCC1453	12:32:44.22	14:11:46.17	-17.9	18.9	35.6 ± 1.4
VCC1528	12:33:51.61	13:19:21.03	-17.5	09.6	47.0 ± 1.4
VCC1549	12:34:14.83	11:04:17.51	-17.3	12.1	36.7 ± 2.3
VCC1695	12:36:54.85	12:31:11.93	-17.7	24.0	24.4 ± 2.2
VCC1861	12:40:58.57	11:11:04.34	-17.9	19.0	31.3 ± 1.5
VCC1895	12:41:51.97	09:24:10.28	-17.0	16.3	23.8 ± 3.0
VCC1910	12:42:08.67	11:45:15.19	-17.9	13.4	37.0 ± 1.2
VCC1912	12:42:09.07	12:35:47.93	-17.9	22.5	36.0 ± 1.5
VCC1947	12:42:56.34	03:40:35.78	-17.6	09.3	48.3 ± 1.3

3 RESULTS

3.1 Derived ages and metallicities

Luminosity-weighted ages and metallicities are estimated using age-sensitive ($H\beta$ and $H\gamma_F$) and metallicity-sensitive (Fe4383, Fe4531, Fe5270, Fe5335, Fe5406, Fe5709, and Mgb) Lick spectral indices (Worthey 1994) measured in the LIS-5 Å system (Vazdekis et al. 2010). For this, we used an MCMC (Markov chain Monte Carlo) code to derive the age and metallicity of the best-fitting MILES single stellar population model.

We estimate the best luminosity weighted age and metallicity from all available index–index combinations by effectively computing the ‘distance’ from our measured indices to all predicted values on the model grids, and finding the age and metallicity combination with the minimum total distance. The age and metallicity values for each index–index diagram and associated uncertainties were derived using 1000 MCMC iteration of the fit. To reduce the effects of the grid discretization, the two relevant parameters (e.g. age and metallicity) were interpolated. Uncertainties were

Table 2. A summary of the indices used.

Telescope	WHT	INT and VLT
Age indicator	$H\gamma_F$	$H\beta$
Metal indicator	Fe4383, Fe4531 Fe5709	Fe4531, Fe5270, Fe5335 Fe 5406, Fe5709, Mgb
Na abundances	NaD	–
Ca abundances	Ca4227	–
Mg abundance	–	Mgb

calculated by performing Monte Carlo simulations, making use of the observational error in each index. In Table 5, we list the best-fitting parameters for ages and metallicities that are determined using combinations of all age sensitive lines and all metal indicators.

Fig. 1 shows index–index plots, where we have restricted the age to the interval 1.0–14.0 Gyr, and the metallicity range from -1.76 to 0.26, which includes the range covered by the galaxies in our

Table 3. Lick spectral indices measured at LIS-5 Å resolution for WHT objects.

Galaxy	Ca4227 (Å)	H γ_F (Å)	Fe4383 (Å)	Fe4531 (Å)	Fe5709 (Å)	NaD (Å)
VCC0033	1.25 ± 0.38	1.55 ± 0.39	2.62 ± 0.85	3.09 ± 0.65	0.60 ± 0.22	0.83 ± 0.373
VCC0170	0.75 ± 0.21	2.43 ± 0.22	1.48 ± 0.51	1.70 ± 0.40	0.48 ± 0.09	1.21 ± 0.173
VCC0308	0.99 ± 0.12	1.69 ± 0.14	2.53 ± 0.32	3.02 ± 0.24	0.85 ± 0.09	1.57 ± 0.125
VCC0389	1.17 ± 0.14	0.33 ± 0.14	3.90 ± 0.29	2.87 ± 0.21	0.99 ± 0.07	1.68 ± 0.095
VCC0397	1.11 ± 0.12	1.33 ± 0.14	3.92 ± 0.31	3.50 ± 0.24	0.94 ± 0.11	1.92 ± 0.136
VCC0437	0.87 ± 0.25	-0.76 ± 0.27	2.49 ± 0.57	2.01 ± 0.41	0.80 ± 0.10	2.08 ± 0.165
VCC0523	1.13 ± 0.07	0.93 ± 0.09	3.25 ± 0.19	3.14 ± 0.15	0.91 ± 0.10	1.50 ± 0.177
VCC0543	1.41 ± 0.13	-0.17 ± 0.16	3.96 ± 0.32	3.23 ± 0.23	0.77 ± 0.06	1.95 ± 0.093
VCC0634	1.21 ± 0.15	0.55 ± 0.16	3.70 ± 0.33	3.05 ± 0.25	0.75 ± 0.13	-
VCC0750	1.09 ± 0.20	0.75 ± 0.21	3.36 ± 0.44	3.00 ± 0.33	0.80 ± 0.08	1.61 ± 0.122
VCC0751	1.62 ± 0.25	-0.23 ± 0.27	4.80 ± 0.53	3.93 ± 0.40	1.16 ± 0.16	-
VCC0781	0.66 ± 0.22	2.74 ± 0.21	1.31 ± 0.49	2.19 ± 0.37	-	-
VCC0794	1.06 ± 0.24	0.43 ± 0.26	2.84 ± 0.55	2.18 ± 0.41	0.62 ± 0.08	1.45 ± 0.117
VCC0917	0.99 ± 0.10	0.41 ± 0.13	3.28 ± 0.27	2.96 ± 0.21	0.65 ± 0.09	1.26 ± 0.129
VCC1010	1.42 ± 0.07	-0.83 ± 0.09	4.49 ± 0.17	3.25 ± 0.13	0.85 ± 0.04	2.33 ± 0.054
VCC1087	1.33 ± 0.10	-0.51 ± 0.12	4.79 ± 0.23	2.98 ± 0.18	0.79 ± 0.08	-
VCC1122	1.11 ± 0.10	0.86 ± 0.12	3.20 ± 0.26	2.52 ± 0.21	0.71 ± 0.20	-
VCC1304	0.81 ± 0.13	1.72 ± 0.15	2.31 ± 0.34	2.60 ± 0.26	0.52 ± 0.07	1.95 ± 0.097
VCC1355	1.39 ± 0.33	0.59 ± 0.35	2.77 ± 0.74	3.06 ± 0.55	0.78 ± 0.10	1.32 ± 0.188
VCC1407	0.83 ± 0.18	0.12 ± 0.20	3.35 ± 0.40	2.81 ± 0.30	0.53 ± 0.08	1.55 ± 0.129
VCC1453	1.52 ± 0.13	-0.43 ± 0.14	4.38 ± 0.29	3.40 ± 0.21	0.99 ± 0.06	2.08 ± 0.065
VCC1528	1.27 ± 0.18	-0.40 ± 0.19	4.49 ± 0.38	3.28 ± 0.28	0.96 ± 0.07	2.33 ± 0.093
VCC1695	1.03 ± 0.09	1.47 ± 0.10	2.82 ± 0.23	2.75 ± 0.18	0.80 ± 0.08	1.63 ± 0.123
VCC1861	1.43 ± 0.11	-0.66 ± 0.14	3.71 ± 0.29	2.87 ± 0.22	0.70 ± 0.10	-
VCC1895	1.09 ± 0.20	0.83 ± 0.23	2.73 ± 0.49	2.75 ± 0.37	0.70 ± 0.10	1.26 ± 0.155

Table 4. Lick spectral indices measured at LIS-5 Å resolution for INT and VLT objects.

Galaxy	Fe4531 (Å)	H β (Å)	Mgb (Å)	Fe5270 (Å)	Fe5335 (Å)	Fe5406 (Å)	Fe5709 (Å)
VCC0021	1.23 ± 0.40	3.98 ± 0.19	0.96 ± 0.23	1.25 ± 0.25	1.52 ± 0.29	0.51 ± 0.23	0.11 ± 0.20
VCC0856	3.35 ± 0.62	2.30 ± 0.29	2.44 ± 0.33	2.38 ± 0.36	1.87 ± 0.41	0.67 ± 0.32	1.39 ± 0.27
VCC0940	2.33 ± 0.17	2.22 ± 0.09	2.64 ± 0.08	2.45 ± 0.09	1.78 ± 0.10	1.30 ± 0.07	...
VCC0990	3.20 ± 0.30	2.81 ± 0.15	2.49 ± 0.17	2.62 ± 0.19	2.29 ± 0.21	1.58 ± 0.16	0.83 ± 0.15
VCC1183	3.49 ± 0.35	2.61 ± 0.16	2.95 ± 0.18	2.82 ± 0.20	2.23 ± 0.23	1.59 ± 0.17	0.95 ± 0.15
VCC1261	2.33 ± 0.21	2.47 ± 0.11	2.19 ± 0.12	2.52 ± 0.13	2.13 ± 0.15	1.47 ± 0.12	0.94 ± 0.11
VCC1431	3.53 ± 0.33	1.95 ± 0.16	3.17 ± 0.18	2.46 ± 0.19	1.93 ± 0.22	1.41 ± 0.17	0.46 ± 0.15
VCC1549	2.72 ± 0.46	1.73 ± 0.22	3.02 ± 0.25	2.85 ± 0.26	2.48 ± 0.30	1.74 ± 0.22	0.99 ± 0.20
VCC1910	3.24 ± 0.33	1.75 ± 0.15	2.82 ± 0.16	2.50 ± 0.18	2.84 ± 0.19	2.06 ± 0.15	0.30 ± 0.13
VCC1912	2.31 ± 0.24	3.66 ± 0.11	1.32 ± 0.13	2.21 ± 0.14	2.30 ± 0.16	1.15 ± 0.13	0.16 ± 0.11
VCC1947	3.26 ± 0.32	1.82 ± 0.15	3.18 ± 0.17	2.99 ± 0.18	2.69 ± 0.20	1.85 ± 0.16	0.94 ± 0.14

sample. We use the solar-scaled theoretical isochrones in the model grids from Vazdekis et al. (2010) in Fig. 1.

For our dEs sample, the measured NaD values are much lower than the model predictions for solar-abundance models (Fig. 2) while ca4227 values are slightly higher than the predicted by models (Fig. 3)

3.2 Elemental abundance ratios

To calculate the abundance ratios $[E/Fe]$ from the indices, we first calculate age and metallicity as described above, assuming that the galaxies can be represented by an SSP model. We then measure the difference between the observed index related to the element E and the index value expected from stellar population models for the age and metallicity that we measure for the galaxy, and divide this difference by the sensitivity of the index to variations in $[E/Fe]$

(equation 1). For Na (NaD) and Mg (Mgb), we use the Na-MILES model of La Barbera et al. (2017) based on Teramo isochrones, with variable Mg and Na abundance ratios, and with a (standard) bimodal IMF with $\Gamma_b = 1.3$. Unfortunately, Mgb was measured only in a few galaxies, those observed with the VLT and the INT. For Ca, we do the same using the Ca4227 index. The problem here is that for this element no stellar population models are available. The only available model, by CvD, has solar metallicity, and a fixed, old, age of 13.5 Gyr, which is different from the ages and metallicities of the objects we discuss here. In this paper, we will use this latter model, but move the analysis and discussion to Appendix A, since we do not know how appropriate this is.

So, for element E based on index i , the elemental abundance ratios were calculated using

$$[E_i/Fe] = \frac{i_{\text{observed}} - i_{\text{model}}}{\frac{\Delta i_{\text{model}}}{\Delta [E_i/Fe]_{\text{model}}}}, \quad (1)$$

Table 5. Elemental abundances, metallicity and ages. Column 1: galaxy name. Column 2 and 3: measurement of [Ca/Fe] and [Na/Fe] for galaxies that are observed with the WHT. Column 4: measurement of [Mg/Fe] for galaxies that are observed using the INT and VLT. Column 5 and 6: metallicity [M/H] and logarithmic ages in Gyr with errors.

Galaxy	[Ca/Fe]	[Na/Fe]	[Mg/Fe]	[Fe/H]	log (age) (Gyr)
VCC0009	0.05	−0.52	–	−1.06 ± 0.15	0.94 ± 0.03
VCC0021	–	–	0.03	−1.17 ± 0.18	0.20 ± 0.07
VCC0033	0.32	−0.57	–	−1.00 ± 0.01	0.83 ± 0.17
VCC0170	0.17	−0.32	–	−1.05 ± 0.08	0.47 ± 0.09
VCC0308	0.14	−0.24	–	−0.40 ± 0.24	0.34 ± 0.04
VCC0389	0.15	−0.23	–	−0.37 ± 0.16	0.70 ± 0.04
VCC0397	0.05	−0.20	–	0.06 ± 0.35	0.23 ± 0.04
VCC0437	0.12	−0.06	–	−0.71 ± 0.01	0.98 ± 0.07
VCC0523	0.17	−0.33	–	−0.19 ± 0.29	0.41 ± 0.03
VCC0543	0.21	−0.17	–	−0.44 ± 0.07	0.83 ± 0.05
VCC0634	0.30	–	–	−0.93 ± 0.35	0.84 ± 0.30
VCC0750	0.13	−0.24	–	−0.47 ± 0.10	0.62 ± 0.06
VCC0751	0.45	–	–	−0.93 ± 0.36	0.85 ± 0.29
VCC0781	0.11	–	–	−0.90 ± 0.24	0.84 ± 0.30
VCC0794	0.25	−0.31	–	−0.81 ± 0.03	0.90 ± 0.08
VCC0856	–	–	0.05	−0.64 ± 0.31	0.92 ± 0.16
VCC0917	0.08	−0.43	–	−0.47 ± 0.12	0.69 ± 0.05
VCC0940	–	–	0.40	−0.97 ± 0.35	0.84 ± 0.29
VCC0990	–	–	0.07	−0.23 ± 0.12	0.43 ± 0.08
VCC1010	0.18	−0.07	–	−0.31 ± 0.10	0.94 ± 0.03
VCC1087	0.35	–	–	−0.94 ± 0.25	0.84 ± 0.30
VCC1122	0.27	–	–	−0.93 ± 0.30	0.85 ± 0.29
VCC1183	–	–	0.15	−0.26 ± 0.02	0.67 ± 0.11
VCC1261	–	–	0.04	−0.33 ± 0.13	0.52 ± 0.06
VCC1304	0.15	0.06	–	−0.68 ± 0.10	0.55 ± 0.07
VCC1355	0.34	−0.32	–	−0.64 ± 0.01	0.75 ± 0.12
VCC1407	0.11	−0.27	–	−0.73 ± 0.07	0.95 ± 0.05
VCC1431	–	–	0.11	−0.49 ± 0.02	1.07 ± 0.06
VCC1453	0.23	−0.15	–	−0.27 ± 0.13	0.76 ± 0.05
VCC1528	0.14	−0.05	–	−0.25 ± 0.05	0.79 ± 0.06
VCC1549	–	–	0.08	−0.41 ± 0.09	1.04 ± 0.09
VCC1695	0.15	−0.21	–	−0.40 ± 0.22	0.39 ± 0.05
VCC1861	0.38	–	–	−0.90 ± 0.57	0.85 ± 0.29
VCC1895	0.22	−0.37	–	−0.77 ± 0.15	0.82 ± 0.11
VCC1910	–	–	0.05	−0.37 ± 0.40	0.93 ± 0.11
VCC1912	–	–	−0.07	−0.07 ± 0.28	0.14 ± 0.01
VCC1947	–	–	−0.09	−0.93 ± 0.47	0.88 ± 0.11

where i_{observed} is the value of the index measured from the observations, i_{model} is the index expected from the model, and E_i is the elemental abundance.

In Table 5, we provide the elemental abundances for each galaxy determined according to the procedure described above. The spectral range covered allowed the measurement of [Ca/Fe] and [Na/Fe] for most galaxies that are observed by WHT, and [Mg/Fe] for some that are observed by INT and VLT. We do not have galaxies for which all three abundance ratios have been measured.

To establish the reliability of these abundance ratios, we made a comparison of the sensitivity of ΔNaD to variations in [Na/Fe] and ΔMgb to variations in [Mg/Fe] between the SSP models of *CvD* and *MILES*. For a meaningful comparison, we have computed some additional α enhancement SSP models for a total metallicity of [M/H] = 0.3 (for [Fe/H] 0.0, from equation 4 of Vazdekis et al. 2012). For the Na comparison, a Na-*MILES* model (La Barbera et al. 2017) is computed for the same age and metallicity as *CvD*.

We find that the Na-*MILES* model gives a slightly larger sensitivity for Na than the one of *CvD* and that we get similar results from

both *CvD* and *MILES* for Mgb. Note, however, that the sensitivities vary considerably when going to lower ages and metallicities.

We report the values of the ΔNaD and ΔMgb variations as a function of these elemental abundance ratios for models with different ages and metallicities in Table 6. When we compare the sensitivities at the same age, we find that the NaD sensitivity generally increases with metallicity, whereas the one for Mgb generally decreases. When one increases the age, both sensitivities tend to increase (see Table 6).

4 DISCUSSION

We present ages, metallicities, and abundance ratios obtained for 37 dEs within an aperture size of $R_c/8$. This aperture size is commonly used in conventional long-slit studies. The radius has been chosen to provide a measure of the stellar populations in the central regions of these galaxies, in a region with a constant relative size. Following the classification of Lisker et al. (2006a,b, 2007), using high-pass filtered Sloan Digital Sky Survey (SDSS; Adelman-McCarthy et al.

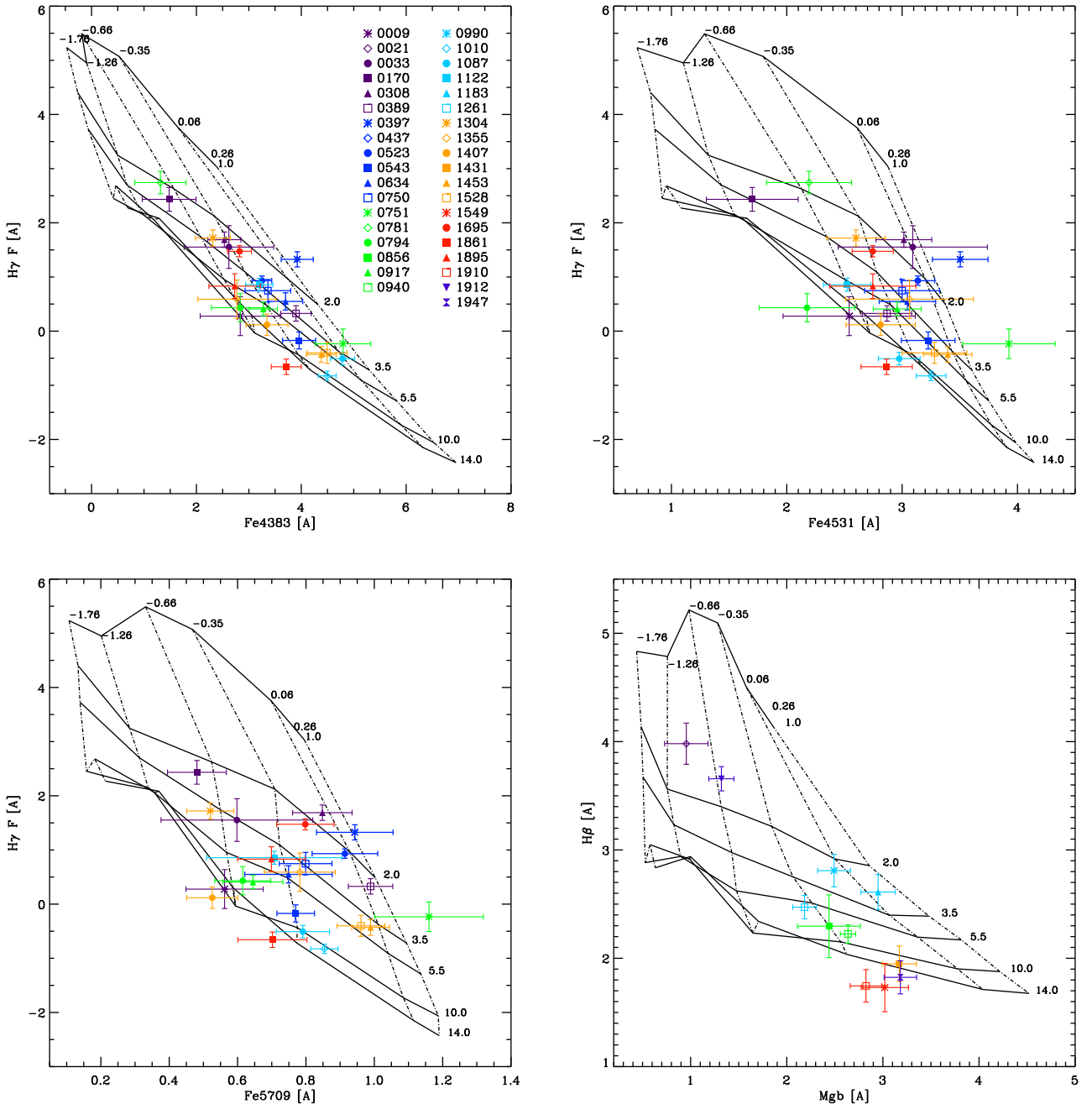


Figure 1. Spectral index–index diagrams used to estimate the stellar populations using solar-scaled theoretical isochrone grids with IMF slope of 1.3 from Vazdekis et al. (2010) in the system LIS 5 Å, solid lines indicate constant age 1.0, 2.0, 3.5, 5.5, 10.0, and 14.0 Gyr, respectively, whereas dotted lines indicate constant $[M/H]$ -1.76 , -1.26 , -0.65 , -0.35 , $+0.06$, and $+0.26$, respectively.

2006), 36 of the galaxies of our sample are classified as nucleated. VCC0021 and VCC1431 are galaxies with large blue core. All the analysis comes from the central regions, in which the nuclear cluster’s light is contributing significantly. The resulting abundance ratios can thus provide insight about the luminosity-weighted stellar population in this region. Although we could have tried to derive two-burst or more complicated SFHs, it would have been very hard with the current low-resolution data to be able to distinguish between a one- or two-burst solution (see e.g. Ryś et al. 2015; Mentz et al. 2016). For that reason, we postpone this to a future paper, in which we analyse spectra at a spectral resolution of $R = 5000$ using the SAMI instrument at the AAT.

One of the main results of this paper is the unusual behaviour of the Na abundances in dEs, when compared with massive ellipticals and Local Group dwarfs. For a sample of quiescent dwarfs with effective velocity dispersion in the range $20\text{--}55\text{ km s}^{-1}$ and with absolute r -band magnitude ranging from -19 to -16 , we find that our sample of dEs is underabundant in Na when compared to the solar neighbourhood (Fig. 4). At the same time, the Mg abundances are around solar. In the following, we try to argue what this means for the evolution of dwarf ellipticals, based on what we know from theory, and observations of individual stars in the Milky Way and the Local Group, and integrated abundance ratios in giant elliptical galaxies. For dwarf ellipticals, such an analysis using integrated

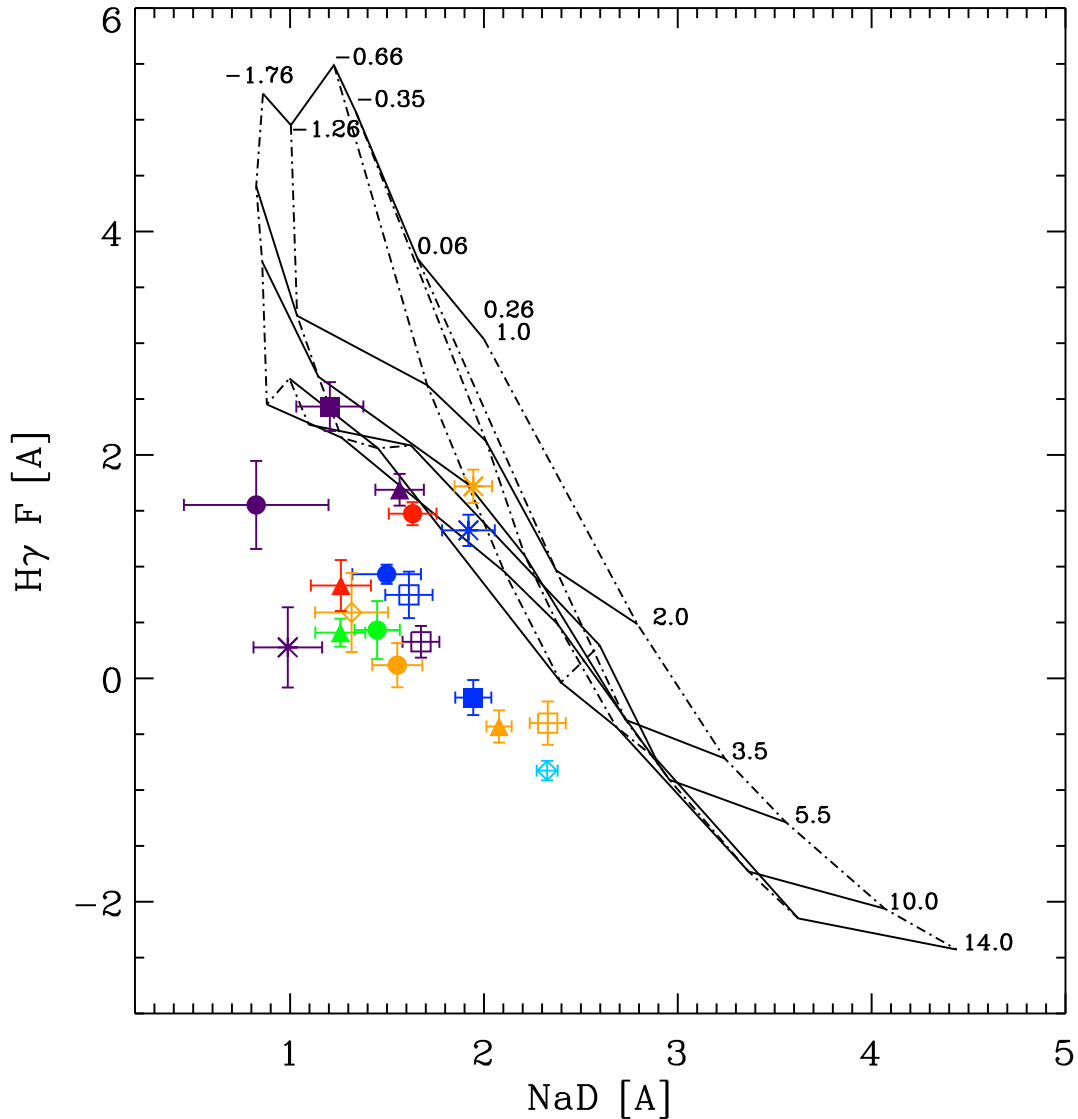


Figure 2. Example of a spectral index–index diagram for $H\gamma_F$ versus NaD , showing that the NaD values are much lower than the predicted by models. Models from Vazdekis et al. 2010. Constant age and $[M/H]$ as in Fig. 1.

light has not been done before, although several papers have tried to derive abundance ratios in giant ellipticals (e.g. Worthey 1998; Yamada et al. 2006; Thomas et al. 2010; Worthey, Ingermann & Serven 2011; Conroy et al. 2014; Spiniello et al. 2014; Smith et al. 2015).

In this paper, we are analysing light elements. It is our current belief that in the most-studied environments the relative abundance $[X/Fe]$ of an element X at low $[Fe/H]$ represents the abundance ratio from only those sources of material processed through the nucleosynthesis channels that were active at very early times, i.e. SN II from core collapse of massive stars, events characteristic of the earliest epochs of star formation (Cohen & Huang 2009). After these early times, $[X/Fe]$ is modified by other sources, such as SN Ia, SN II, AGB stars, novae, etc., and also by the accretion of primordial material and of galactic winds. This gives a knee-like pattern in the relation between $[X/Fe]$ and $[Fe/H]$, of which the position of the bend is determined by the delay time between the core collapse SN II and the other processes. This delay depends on various parameters (IMF, star formation efficiency, the rate of mass-loss in stars, and

the rate of accretion of primordial gas consisting mostly of H), as well as on the element production yields (e.g. Greggio, Renzini & Daddi 2008). These processes lead to the characteristic knee in the Milky Way, where low metallicity halo stars generally have $[Mg/Fe]$ values around 0.4, a value reached by SN II enrichment only, going down to solar mass disc stars, with $[Mg/Fe]$ values around solar, an equilibrium values reached when all processes have contributed. From these solar abundance ratios in the disc of our Milky Way, one can then conclude that star formation has been taken place on long time-scales compared to the halo.

We will now have a more detailed look at the individual abundance ratios.

4.1 Na abundances

Na is believed to be made in the interiors of massive stars and to depend on the neutron excess, which in turn depends on the initial heavy element abundance in the star. Na thus has both a primary and a secondary nucleosynthesis channel (Arnett 1971; Clayton 2003).

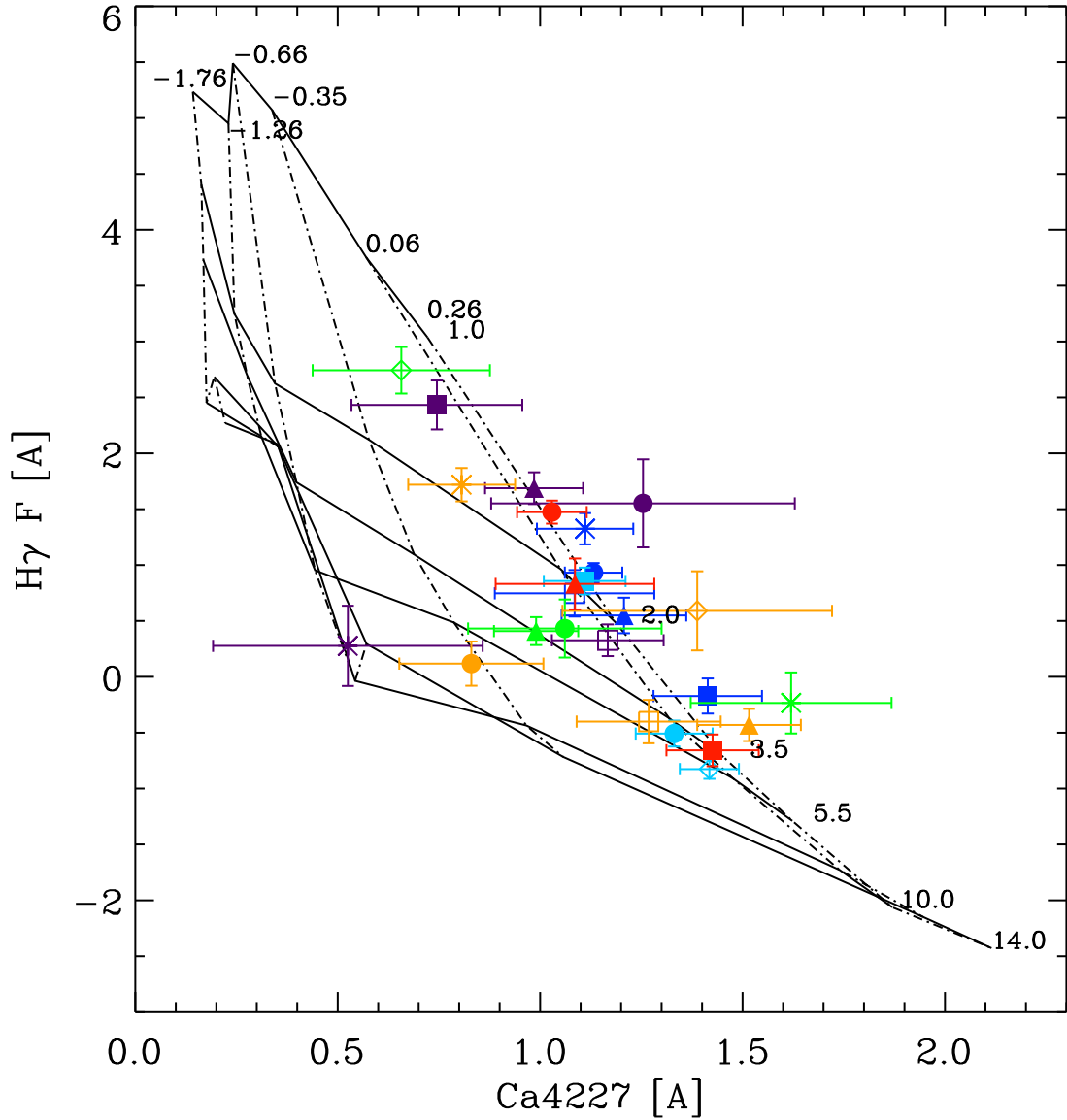


Figure 3. Example of spectral index–index diagram for $H\gamma F$ versus $Ca4227$, showing that the $Ca4227$ values are slightly higher than predicted by models. Models from Vazdekis et al. 2010. Constant age and $[M/H]$ as in Fig. 1.

Table 6. Comparison of MILES and CvD model predictions (column 1) with varying metallicity (column 2) and age (column 3). Columns 4 and 5: ΔNaD variations in $[Na/Fe]_*$, $\Delta Ca4227$ variations in $[Ca/Fe]_*$ and $\Delta Mg b$ variations in $[Mg/Fe]_*$ based on the models shown in col.1

Model (*)	$[M/H]$ (dex)	Age (Gyr)	$\frac{\Delta NaD_*}{\Delta [Na/Fe]_*}$	$\frac{\Delta Mg b_*}{\Delta [Mg/Fe]_*}$	$\frac{\Delta Ca4227_*}{\Delta [Ca/Fe]_*}$
CvD	0.00	13.50	3.085	4.260	2.790
MILES	0.06	14.00	3.547	4.350	–
MILES	–0.35	1.00	0.973	3.133	–
MILES	–0.35	7.00	2.317	4.830	–
MILES	–0.35	14.00	2.683	5.609	–
MILES	0.06	1.00	1.453	3.009	–
MILES	0.06	7.00	3.167	3.298	–
MILES	0.26	1.00	1.583	3.463	–
MILES	0.26	7.00	3.380	3.336	–
MILES	0.26	14.00	3.830	3.768	–

Ni is assumed to originate predominantly from SNe Ia. However, the production of Ni might also be linked to the production of Na in SNe II (Thielemann, Hashimoto & Nomoto 1990; Timmes, Woosley & Weaver 1995). The amount of Na produced is controlled by the neutron excess, where ^{23}Na is the only stable neutron rich isotope produced in significant quantity during the C and O burning stage. The production of Ni depends on the neutron excess and the neutron excess will depend primarily on the amount of ^{23}Na previously produced. Hence, an Na–Ni correlation is expected when the chemical enrichment is dominated by SNe II. The advent of the SNe Ia explosions can break (or flatten) this relationship, as Ni is produced without Na in the standard model of SN Ia (e.g. Iwamoto et al. 1999). Since the neutron excess is strongly metallicity-dependent, this could explain the low $[Na/Fe]$ that are being found for the Fornax dwarf (Letarte et al. 2010). At the same time, it would explain the high values in giant ellipticals (see later).

It is important to mention that the abundance ratios found here are very different from those in other stellar systems, most massive

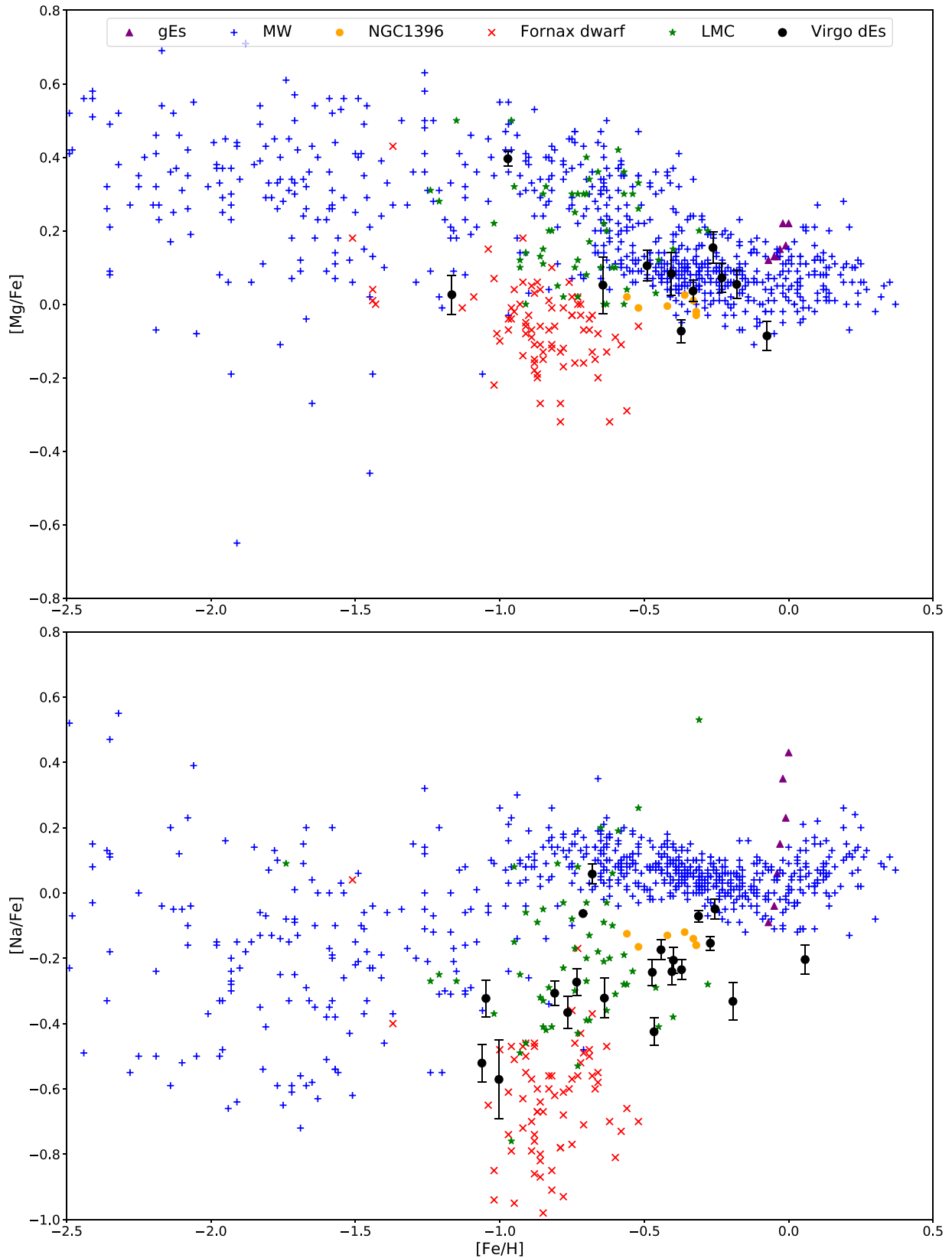


Figure 4. Mg and Na abundances as a function of metallicity $[Fe/H]$. Blue pluses are the Milky Way stars from Venn et al. (2004), red crosses are from the Fornax local dwarf from Letarte et al. (2010) and Shetrone et al. (2003), green asterisks are the LMC red giants from Pompéia et al. (2008), purple triangles are giant ellipticals from Conroy et al. (2014), orange circles are various radial bins of the NGC1396 in the Fornax cluster from Mentz et al. (2016), and black circles are the dEs in Virgo cluster analysed here.

Galactic globular clusters, and giant elliptical galaxies. In most massive globular clusters, a strong Na–O anticorrelation is observed in the RGB stars (Kraft 1994, and see reviews of Carretta 2016; Gratton et al. 2001). For these stars, Oxygen is depleted, and Na enhanced, just like N. Since this effect is not seen in the interior of the presently observed GC low-mass stars, it is thought that this is a second generation (SG) enrichment effect from massive stars, which have enhanced their Na-abundance during C-burning through the NeNa cycle (Langer, Hoffman & Sneden 1993). It is thought that SG stars are formed by nuclear ejecta processed in the most massive first generation (FG) stars, diluted with different amounts of unprocessed gas, generating a number of anticorrelations, including the one of Na and O. This process, as far as we know, does not take place in the halo of our Milky Way, and in field stars of Local Group galaxies. In this paper, we see that this is also not the case in field stars of dwarf ellipticals in nearby galaxy clusters.

Four strong Na absorption features can be found in the optical and NIR wavelength range: NaD (5890 and 5896 Å), NaI 0.82 (8183 and 8195 Å), NaI1.14 (11400 Å), and NaI2.21 (22100 Å). The equivalent widths (EWs) of NaD were studied first by O’Connell (1976) and Peterson (1976), where they reported that NaD was much stronger than expected from Ca and Fe indices in giant ETGs. Spiniello, Trager & Koopmans (2015) reported that the NaD feature is very sensitive to [Na/Fe] variations, whereas the NaI index seems to depend mainly on the IMF (e.g. Vazdekis et al. 2012). La Barbera et al. (2017) perform detailed fits to all four Na-lines in a number of giant ellipticals, and find that both [Na/Fe] needs to be considerably larger than solar, and the IMF-slope needs to be dwarf-enhanced (Smith et al. 2015). For dwarf ellipticals, however, there are no indications that the IMF-slope is different from our Galaxy (Mentz et al. 2016). Here, we find the behaviour that [Na/Fe] is lower than solar, opposite to the behaviour in giant ellipticals.

Remarkable is the strong trend between [Na/Fe] and [Fe/H], already mentioned by Mentz et al. (2016) when joining the Fornax dwarf with our dwarf ellipticals and the giant ellipticals. For [Fe/H] values of ~ -0.8 , very low [Na/Fe] values are obtained of ~ -0.6 – -0.8 in the Fornax dwarf. This contrasts with the high, positive [Na/Fe] values that are found in giant ellipticals. Such a strong correlation is what you could expect if the Na-abundance depends strongly on the neutron excess, or equivalently, the metallicity.

4.2 Abundance ratios and the formation of dEs

In this paper, we find [Mg/Fe] values that are very close to solar (the mean value of the [Mg/Fe] is 0.07), or slightly larger. [Na/Fe] is (the mean value of the [Na/Fe] is -0.25), however, considerably lower than solar.

When comparing to stellar populations that show similar abundance patterns, there are not many, but one could consider the younger, and more metal-rich stellar populations in the centre of the Fornax Dwarf galaxy, published by Letarte et al. (2010). The majority of those stars are 1–4 Gyr old, and have unusually low [Mg/Fe], [Ca/Fe], and [Na/Fe] compared to the Milky Way stellar populations at the same [Fe/H], and are therefore at the end of their chemical evolution. The difficulty is that, although [Mg/Fe] is approximately solar for these stars, [Ca/Fe] lies considerably below this value. Letarte et al. (2010) hypothesize that this means that a large fraction of Ca and Ti is produced in processes that do not produce much Mg, such in SNe Ia. In this way, the low [Ca/Fe] and [Ti/Fe] could be a consequence of the low metallicity of their progenitors compared to the Milky Way. At the same time, [Na/Fe]

is found to be rather low (between -0.9 and -0.4), but correlating strongly with [Ni/Fe] (Nissen & Schuster 1997, 2009).

For the dwarf ellipticals in Virgo analysed in this paper, we conclude, analogous to Letarte et al. (2010), that the low [Mg/Fe] values (w.r.t. the thick disc of the Milky Way and giant ellipticals) show that the galaxies have undergone a considerable amount of chemical evolution. This means that the galaxies are not uniformly old, but have extended SFHs, similar to many of the Local Group galaxies. [Na/Fe] is lower than solar, but still higher than in the Fornax dwarf. This is expectable, since the metallicities of the dwarf ellipticals in Virgo are a bit larger, resulting in a larger neutron excess and higher Na-abundances.

For dEs, we find that (a) [Mg/Fe] ~ 0 , and (b) [Na/Fe] < 0 . Result (a) implies that star formation is slow, like in the Milky Way disc. Result (b) is consistent with the same formation mechanism. Just like the stars of Letarte et al. (2010) in the centre of the Fornax dwarf galaxy, the stars in the dEs have undergone a considerable amount of enrichment and have an extended SFH. The dependence of [Na/Fe] on the neutron-excess causes [Na/Fe] to be below 0, since for the Virgo dwarfs, [Fe/H] is lower than solar (~ -0.5). The extended SFH then could also cause considerable Ca-enrichment, leading for the dwarf ellipticals to larger [Ca/Fe] values, since they accrete material from the metal-rich cluster environment, rather than the Fornax dwarf, which accretes more pristine gas in the Local Group, which causes lower [Ca/Fe] ratios. An important clue might be strong correlation between [Na/Fe] and [Fe/H], when one considers Local Group dwarf galaxies like Fornax and the LMC, dwarf elliptical galaxies, the disc of the Milky Way, and the centres of giant elliptical galaxies. All this could be due to Na-yields that depend strongly on metallicity. The abundance of sodium influences the electron pressure so that the strength of many other features is affected. For example, Conroy & van Dokkum (2012) show that for massive galaxies, an increase in the sodium abundance causes a decrease in the abundance of Ca II, which causes a decrease in the EW of CaT. Increasing the sodium abundance can mimic the effects of a more bottom-heavy IMF. For dwarfs, however, we see a different behaviour comparing Ca and Na, although there is no evidence that the IMF is responsible here. And also, for the LMC, both [Na/Fe] and [Ca/Fe] have the same sign, implying that another parameter has to be responsible for the difference between LMC and the dEs, presumably the SFH. However, with this considerable (~ 0.2) difference in [Ca/Fe] between the LMC and the dEs, it is not so obvious that objects like the LMC should be the progenitors of dEs, unless Ca-enrichment by SN Ia in the cluster environment was particularly effective.

What is clear is that the abundance ratio pattern in dwarf ellipticals is very different from that in massive Galactic globular clusters, which show enhanced [Na/Fe], a strong Na–O anticorrelation etc. in many stars. It is of course still possible that a fraction of the stars display these effects, but that fraction is so small that it cannot be detected in integrated light. This difference probably indicates that star formation time-scales in dwarf ellipticals are long, on the order of Gyr, since these globular clusters must have been formed on very small time-scales, with their ages being so large (Gratton et al. 2001).

5 CONCLUSIONS

(i) In this paper, we determine abundance ratios of a sample 37 dEs in the Virgo cluster as a part of the SMAKCED project. This sample is representative of the analysis of the kinematic properties

(Toloba et al. 2014a) and also all morphological sub-classes found by Lisker et al. (2006a,b, 2007).

(ii) We use optical spectroscopy to measure a total of 23 Lick indices in the LIS-5 Å flux calibrated system and apply the MILES models to interpret them. We derive new age and metallicity estimates for these galaxies. Taking advantage of high resolution spectral data, we are able to calculate the abundance ratios of Na and Mg using the models of MILES.

(iii) We find the unusual behaviour that [Na/Fe] is underabundant w.r.t. solar. This is opposite to what is found in massive giant elliptical galaxies. We also find that dEs fall on a relatively tight relation between [Na/Fe] and [Fe/H], which we recently presented in Mentz et al. (2016), including Local Group dwarf galaxies, the Milky Way, and giant elliptical galaxies. From our results, we try to sketch a possible scenario for the evolution of dEs in the Virgo cluster. We find that dEs show disc-like SFHs, favouring them to originate from star-forming spirals or dwarfs.

(iv) Na-yields appear to be very metal-dependent, in agreement with studies of giant ellipticals, probably due to the large dependence on the neutron-excess in stars.

(v) We conclude that dEs have undergone a considerable amount of chemical evolution, they are therefore not uniformly old, but have extended SFHs, similar to many of the Local Group galaxies.

ACKNOWLEDGEMENTS

We thank an anonymous referee for his critical comments, helping to improve the paper. We also thank to F. La Barbera for kindly providing the new models. The research was supported by The Scientific and Technological Research Council of Turkey (TUBITAK) under project number 1059B141401204 and 1649B031406124. RFP, AV, and JF-B acknowledge support from grant AYA2016-77237-C3-1-P from the Spanish Ministry of Economy and Competitiveness (MINECO). Paudel acknowledges the support by Samsung Science & Technology Foundation under Project Number SSTF-BA1501-0.

REFERENCES

Adelman-McCarthy J. K. et al., 2006, *ApJS*, 162, 38
 Arnott W. D., 1971, *ApJ*, 166, 153
 Barazza F. D., Binggeli B., Jerjen H., 2002, *A&A*, 391, 823
 Binggeli B., Sandage A., Tammann G. A., 1988, *ARA&A*, 26, 509
 Binggeli B., Popescu C. C., Tammann G. A., 1993, *A&AS*, 98, 275
 Blanton M. R., Eisenstein D., Hogg D. W., Schlegel D. J., Brinkmann J., 2005, *ApJ*, 629, 143
 Boselli A., Gavazzi G., 2006, *PASP*, 118, 517
 Boselli A., Gavazzi G., 2014, *A&AR*, 22, 74
 Boselli A. et al., 2014, *A&A*, 570, A69
 Bruzual G., Charlot S., 2003, *MNRAS*, 344, 1000
 Cardiel N., 1999, PhD thesis, Universidad Complutense de Madrid, Spain
 Carretta E., 2016, preprint ([arXiv:1611.04728](https://arxiv.org/abs/1611.04728))
 Cenarro A. J., Gorgas J., Vazdekis A., Cardiel N., Peletier R. F., 2003, *MNRAS*, 339, L12
 Chilingarian I. V., 2009, *MNRAS*, 394, 1229
 Cid Fernandes R., Mateus A., Sodré L., Stasińska G., Gomes J. M., 2005, *MNRAS*, 358, 363
 Clayton D. D., 2003, *Ap&SS*, 285, 353
 Cohen J. G., Huang W., 2009, *ApJ*, 701, 1053
 Cole S., Lacey C. G., Baugh C. M., Frenk C. S., 2000, *MNRAS*, 319, 168
 Conroy C., van Dokkum P., 2012, *ApJ*, 747, 69
 Conroy C., Graves G. J., van Dokkum P. G., 2014, *ApJ*, 780, 33 (CvD)
 De Rijcke S., Dejonghe H., Zeilinger W. W., Hau G. K. T., 2003, *A&A*, 400, 119
 den Brok M. et al., 2011, *MNRAS*, 414, 3052
 Faber S. M., Friel E. D., Burstein D., Gaskell C. M., 1985, *ApJS*, 57, 711

Ferrarese L. et al., 2006, *ApJS*, 164, 334
 Frenk C. S., White S. D., Davis M., Efstathiou G., 1988, *ApJ*, 327, 507
 Gavazzi G., Fumagalli M., Cucciati O., Boselli A., 2010, *A&A*, 517, A73
 Geha M., Guhathakurta P., van der Marel R. P., 2002, *AJ*, 124, 3073
 Geha M., Guhathakurta P., van der Marel R. P., 2003, *AJ*, 126, 1794
 Geha M., Blanton M. R., Yan R., Tinker J. L., 2012, *ApJ*, 757, 85
 Gorgas J., Faber S. M., Burstein D., Gonzalez J. J., Courteau S., Prosser C., 1993, *ApJS*, 86, 153
 Gorgas J., Pedraz S., Guzmán R., Cardiel N., González J. J., 1997, *ApJ*, 481, L19
 Graham A. W., Guzmán R., 2003, *AJ*, 125, 2936
 Gratton R. G. et al., 2001, *A&A*, 369, 87
 Greggio L., Renzini A., Daddi E., 2008, *MNRAS*, 388, 829
 Gunn J. E., Gott J. R., III, 1972, *ApJ*, 176, 1
 Iwamoto K., Brachwitz F., Nomoto K., Kishimoto N., Umeda H., Hix W. R., Thielemann F.-K., 1999, *ApJS*, 125, 439
 Janz J., Lisker T., 2008, *ApJ*, 689, L25
 Janz J., Lisker T., 2009, *ApJ*, 696, L102
 Janz J. et al., 2012, *ApJ*, 745, L24
 Janz J. et al., 2014, *ApJ*, 786, 105
 Jerjen H., Kalnajs A., Binggeli B., 2000, *A&A*, 358, 845
 Koleva M., de Rijcke S., Prugniel P., Zeilinger W. W., Michielsen D., 2009, *MNRAS*, 396, 2133
 Koleva M., Prugniel P., de Rijcke S., Zeilinger W. W., 2011, *MNRAS*, 417, 1643
 Kormendy J., 1985, *ApJ*, 295, 73
 Kraft R. P., 1994, *PASP*, 106, 553
 La Barbera F., Vazdekis A., Ferreras I., Pasquali A., Allende Prieto C., Röck B., Aguado D. S., Peletier R. F., 2017, *MNRAS*, 464, 3597
 Lacey C., Cole S., 1993, *ASP Conf. Ser.*, Vol. 51, *Observational Cosmology*. Astron. Soc. Pac., San Francisco, p. 192
 Langer G. E., Hoffman R., Sneden C., 1993, *PASP*, 105, 301
 Letarte B. et al., 2010, *A&A*, 523, A17
 Lin D. N. C., Faber S. M., 1983, *ApJ*, 266, L21
 Lisker T., Grebel E. K., Binggeli B., 2006a, *AJ*, 132, 497
 Lisker T., Glatt K., Westera P., Grebel E. K., 2006b, *AJ*, 132, 2432
 Lisker T., Grebel E. K., Binggeli B., Glatt K., 2007, *ApJ*, 660, 1186
 Maraston C., 2005, *MNRAS*, 362, 799
 Maraston C., Nieves Colmenárez L., Bender R., Thomas D., 2009, *A&A*, 493, 425
 McWilliam A., 1997, *ARA&A*, 35, 503
 Mei S. et al., 2007, *ApJ*, 655, 144
 Mentz J. J. et al., 2016, *MNRAS*, 463, 2819
 Michielsen D., De Rijcke S., Dejonghe H., Zeilinger W. W., Hau G. K. T., 2003, *ApJ*, 597, L21
 Michielsen D. et al., 2008, *MNRAS*, 385, 1374
 Moore B., Lake G., Katz N., 1998, *ApJ*, 495, 139
 Nelan J. E., Smith R. J., Hudson M. J., Wegner G. A., Lucey J. R., Moore S. A. W., Quinney S. J., Suntzeff N. B., 2005, *ApJ*, 632, 137
 Nissen P. E., Schuster W. J., 1997, *A&A*, 326, 751
 Nissen P. E., Schuster W. J., 2009, in Andersen J., Bland-Hawthorn J., Nordström B., eds, *Proc. IAU Symp. Vol. 254, The Galaxy Disk in Cosmological Context*. Cambridge Univ. Press, Cambridge, p. 103
 O'Connell R. W., 1976, *ApJ*, 206, 370
 Ocvirk P., Pichon C., Lançon A., Thiébaud E., 2006, *MNRAS*, 365, 46
 Paudel S., Lisker T., Kuntschner H., Grebel E. K., Glatt K., 2010, *MNRAS*, 405, 800
 Pedraz S., Gorgas J., Cardiel N., Sánchez-Blázquez P., Guzmán R., 2002, *MNRAS*, 332, L59
 Peterson R. C., 1976, *ApJ*, 210, L123
 Pompéia L. et al., 2008, *A&A*, 480, 379
 Prochaska L. C., Rose J. A., Schiavon R. P., 2005, *AJ*, 130, 2666
 Ryś A., Falcón-Barroso J., van de Ven G., 2013, *MNRAS*, 428, 2980
 Ryś A., van de Ven G., Falcón-Barroso J., 2014, *MNRAS*, 439, 284
 Ryś A., Koleva M., Falcón-Barroso J., Vazdekis A., Lisker T., Peletier R., van de Ven G., 2015, *MNRAS*, 452, 1888
 Saglia R. P., Maraston C., Thomas D., Bender R., Colless M., 2002, *ApJ*, 579, L13
 Schiavon R. P., 2007, *ApJS*, 171, 146

- Shetrone M., Venn K. A., Tolstoy E., Primas F., Hill V., Kaufer A., 2003, *AJ*, 125, 684
- Simien F., Prugniel P., 2002, *A&A*, 384, 371
- Skillman E. D., Kennicutt R. C., Hodge P. W., 1989, *ApJ*, 347, 875
- Smith R. J., Alton P., Lucey J. R., Conroy C., Carter D., 2015, *MNRAS*, 454, L71
- Spiniello C., Trager S., Koopmans L. V. E., Conroy C., 2014, *MNRAS*, 438, 1483
- Spiniello C., Trager S. C., Koopmans L. V. E., 2015, *ApJ*, 803, 87
- Springel V. et al., 2005, *Nature*, 435, 629
- Sybilka A. et al., 2017, *MNRAS*, 470, 815
- Thielemann F.-K., Hashimoto M.-A., Nomoto K., 1990, *ApJ*, 349, 222
- Thomas D., Maraston C., Bender R., 2003, *MNRAS*, 343, 279
- Thomas D., Maraston C., Bender R., Mendes de Oliveira C., 2005, *ApJ*, 621, 673
- Thomas D., Maraston C., Schawinski K., Sarzi M., Silk J., 2010, *MNRAS*, 404, 1775
- Timmes F. X., Woosley S. E., Weaver T. A., 1995, *ApJS*, 98, 617
- Toloba E. et al., 2009, *ApJ*, 707, L17
- Toloba E., Boselli A., Cenarro A. J., Peletier R. F., Gorgas J., Gil de Paz A., Muñoz-Mateos J. C., 2011, *A&A*, 526, A114
- Toloba E. et al., 2014a, *ApJS*, 215, 17 (T14)
- Toloba E. et al., 2014b, *ApJ*, 783, 120
- Toloba E. et al., 2015, *ApJ*, 799, 172
- Tolstoy E., Hill V., Tosi M., 2009, *ARA&A*, 47, 371
- Travaglio C., Hillebrandt W., Reinecke M., Thielemann F.-K., 2004, *A&A*, 425, 1029
- van Zee L., Barton E. J., Skillman E. D., 2004, *AJ*, 128, 2797
- Vazdekis A., 1999, *ApJ*, 513, 224
- Vazdekis A., Peletier R. F., Beckman J. E., Casuso E., 1997, *ApJS*, 111, 203
- Vazdekis A., Trujillo I., Yamada Y., 2004, *ApJ*, 601, L33
- Vazdekis A., Sánchez-Blázquez P., Falcón-Barroso J., Cenarro A. J., Beasley M. A., Cardiel N., Gorgas J., Peletier R. F., 2010, *MNRAS*, 404, 1639
- Vazdekis A., Ricciardelli E., Cenarro A. J., Rivero-González J. G., Díaz-García L. A., Falcón-Barroso J., 2012, *MNRAS*, 424, 157
- Venn K. A., Irwin M., Shetrone M. D., Tout C. A., Hill V., Tolstoy E., 2004, *AJ*, 128, 1177
- Walcher C. J., Coelho P., Gallazzi A., Charlot S., 2009, *MNRAS*, 398, L44
- White S. D., Frenk C. S., 1991, *ApJ*, 379, 52
- White S. D., Rees M. J., 1978, *MNRAS*, 183, 341
- Worthey G., 1994, *ApJS*, 95, 107
- Worthey G., 1998, *PASP*, 110, 888
- Worthey G., Ottaviani D. L., 1997, *ApJS*, 111, 377
- Worthey G., Faber S. M., Gonzalez J. J., 1992, *ApJ*, 398, 69
- Worthey G., Faber S. M., Gonzalez J. J., Burstein D., 1994, *ApJS*, 94, 687
- Worthey G., Ingermann B. A., Servén J., 2011, *ApJ*, 729, 148
- Yamada Y., Arimoto N., Vazdekis A., Peletier R. F., 2006, *ApJ*, 637, 200

APPENDIX A: CA ABUNDANCES

Given the fact that the conversion between Ca4227 and [Ca/Fe] is more uncertain than the ones between NaD and [Na/Fe] and between Mgb and [Mg/Fe], we have put the discussion of the Ca abundances in the appendix.

For our dEs sample, the measured Ca4227 values are slightly higher than the model predictions for solar-abundance models (Fig. 3), implying that Ca is slightly overabundant in dEs. One might get a very rough idea about the values of [Ca/Fe] when using the only available models, those by Cvd for old ages and solar metallicities, to convert Ca4227 to [Ca/Fe]. Although we know that these models are inaccurate, since they must depend on age and metallicity (see the MILES ones), they can serve here to give a crude idea. Using this calibration, Fig. A1 shows that [Ca/Fe] is a bit larger than in the Milky Way disc, but lower than in the thick disc and halo. An interpretation of these high values could be that SN Ia's are partially responsible for the Ca-enrichment (see Travaglio et al. 2004 and above).

Previous abundance measurements of Ca (Michielsen et al. 2003) in dEs show two groups: the ones with CaT* $\sim 7 \text{ \AA}$, higher than expected for solar abundance ratio models, and a sample of three objects with CaT* $\sim 5 \text{ \AA}$. Such lower values could be obtained by having a range in ages, while including some very young objects. The higher values of 7 \AA , however, can only be explained by [Ca/Fe] values that are somewhat larger than solar, consistent with this paper. Our results are also consistent with the line strengths in the Fornax cluster dwarf NGC 1396 (Mentz et al. 2016). Such high [Ca/Fe] values are not seen in giant ellipticals, where the CaT* index is lower than expected from stellar population models with solar abundance ratios (Saglia et al. 2002; Cenarro et al. 2003). Although the latter can be explained by a bottom-heavy IMF, a much easier and more natural explanation would be in [Ca/Fe] < 0 for such galaxies (Cenarro et al. 2003, see also Conroy & van Dokkum 2012). For dEs, the CaT* values are so high that IMF-slopes steeper than Salpeter are excluded (Mentz et al. 2016), so solar or super-solar [Ca/Fe] values are unavoidable. Note, however, the difference between the dEs and the LMC, which has much lower [Ca/Fe] values, but a similar metallicity. We argue that the difference is due to the enrichment by SN Ia and different SFHs.

Prochaska, Rose & Schiavon (2005) suggested that a CN band might be affecting the Ca4227 index in giant ellipticals, but since dEs do not show strong CN bands, the Ca abundance can be measured reliably from the Ca4227 index (Vazdekis et al. 1997).

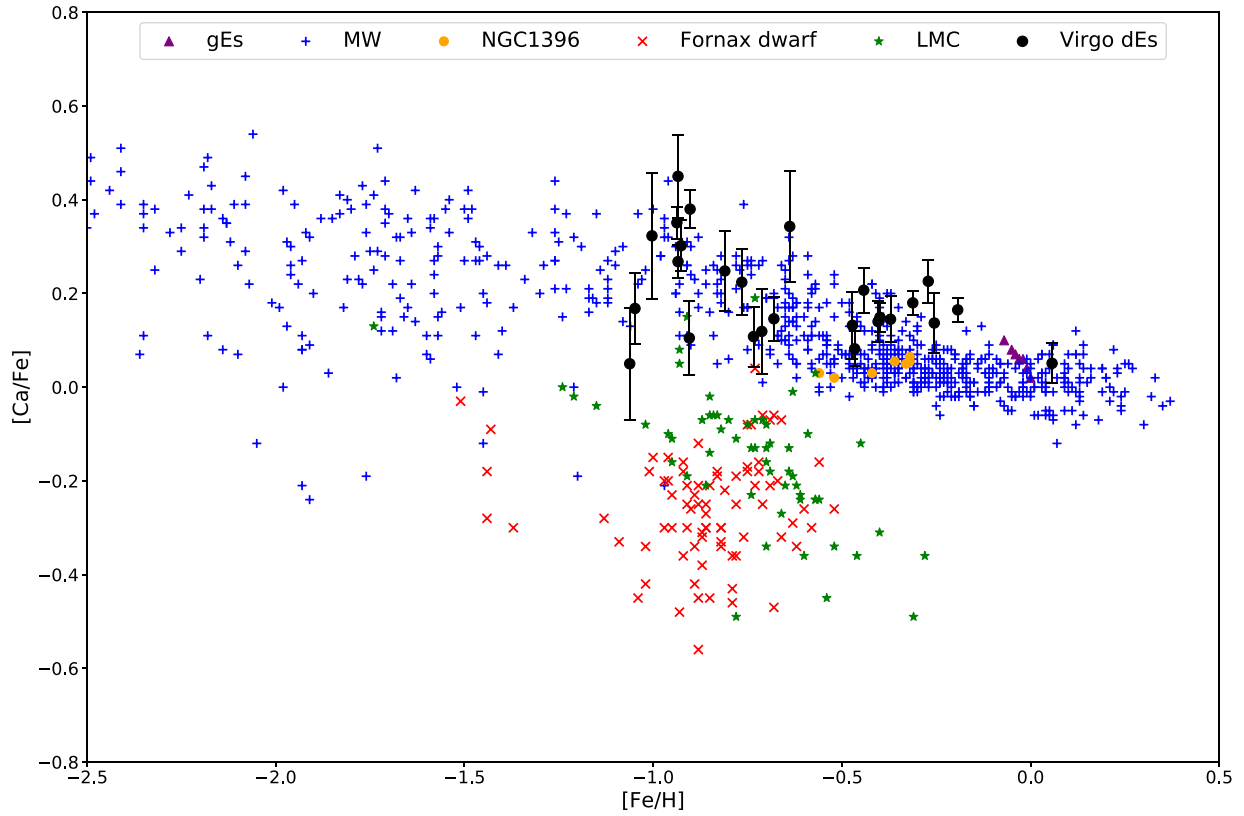


Figure A1. Ca abundances as a function of metallicity [Fe/H]. Description of the points: as in Fig. 4.

This paper has been typeset from a \LaTeX file prepared by the author.